

Insights on multivariate updates of physical and biogeochemical ocean variables using an Ensemble Kalman Filter and an idealized model of upwelling



Liuqian Yu^{a,*}, Katja Fennel^a, Laurent Bertino^b, Mohamad El Gharamti^{b,c}, Keith R. Thompson^a

^a Department of Oceanography, Dalhousie University, Halifax, Nova Scotia B3H 4J1, Canada

^b Nansen Environmental and Remote Sensing Center, Bergen, Norway

^c National Center for Atmospheric Research, Boulder, Colorado, USA

ARTICLE INFO

Keywords:

Ensemble Kalman Filter
Multivariate updates
Coupled physical–biogeochemical ocean model

ABSTRACT

Effective data assimilation methods for incorporating observations into marine biogeochemical models are required to improve hindcasts, nowcasts and forecasts of the ocean's biogeochemical state. Recent assimilation efforts have shown that updating model physics alone can degrade biogeochemical fields while only updating biogeochemical variables may not improve a model's predictive skill when the physical fields are inaccurate. Here we systematically investigate whether multivariate updates of physical and biogeochemical model states are superior to only updating either physical or biogeochemical variables. We conducted a series of twin experiments in an idealized ocean channel that experiences wind-driven upwelling. The forecast model was forced with biased wind stress and perturbed biogeochemical model parameters compared to the model run representing the “truth”. Taking advantage of the multivariate nature of the deterministic Ensemble Kalman Filter (DEnKF), we assimilated different combinations of synthetic physical (sea surface height, sea surface temperature and temperature profiles) and biogeochemical (surface chlorophyll and nitrate profiles) observations. We show that when biogeochemical and physical properties are highly correlated (e.g., thermocline and nutricline), multivariate updates of both are essential for improving model skill and can be accomplished by assimilating either physical (e.g., temperature profiles) or biogeochemical (e.g., nutrient profiles) observations. In our idealized domain, the improvement is largely due to a better representation of nutrient upwelling, which results in a more accurate nutrient input into the euphotic zone. In contrast, assimilating surface chlorophyll improves the model state only slightly, because surface chlorophyll contains little information about the vertical density structure. We also show that a degradation of the correlation between observed subsurface temperature and nutrient fields, which has been an issue in several previous assimilation studies, can be reduced by multivariate updates of physical and biogeochemical fields.

1. Introduction

With the rapid expansion of ocean observing platforms, which now provide a wealth of observations, and growing numerical model capabilities, effective ways of combining observations and dynamic models through data assimilation (DA) are needed. While DA techniques and methodologies are well developed in meteorology and physical oceanography (e.g., Ghil and Malanotte-Rizzoli, 1991; Houtekamer and Mitchell, 1998, 2001; Kalnay, 2003), their applications in marine biogeochemical models are less mature, but actively developing (see reviews of biogeochemical state estimation in Gregg, 2008; Edwards et al., 2015, and state-parameter estimation in Gharamti et al., 2017a,

b). Biogeochemical data assimilation falls into two general categories, the optimization of biogeochemical model parameters through minimization of a cost function (e.g., Fennel et al., 2001; Friedrichs et al., 2007; Kuhn et al., 2015) and updates to the biogeochemical model state by incorporating available observations sequentially (e.g., Eknes and Evensen, 2002; Natvik and Evensen, 2003; Ciavatta et al., 2011; Hu et al., 2012; Ford et al., 2012; Mattern et al., 2013; Ford and Barciela, 2017). Recent efforts have shown that model parameters can also be updated sequentially along with the model state variables (e.g., Simon et al., 2015; Gharamti et al., 2017a, b).

For biogeochemical state estimation, efforts have primarily been made in assimilating satellite ocean color observations, predominantly

* Corresponding author.

E-mail address: liuqian.yu@dal.ca (L. Yu).

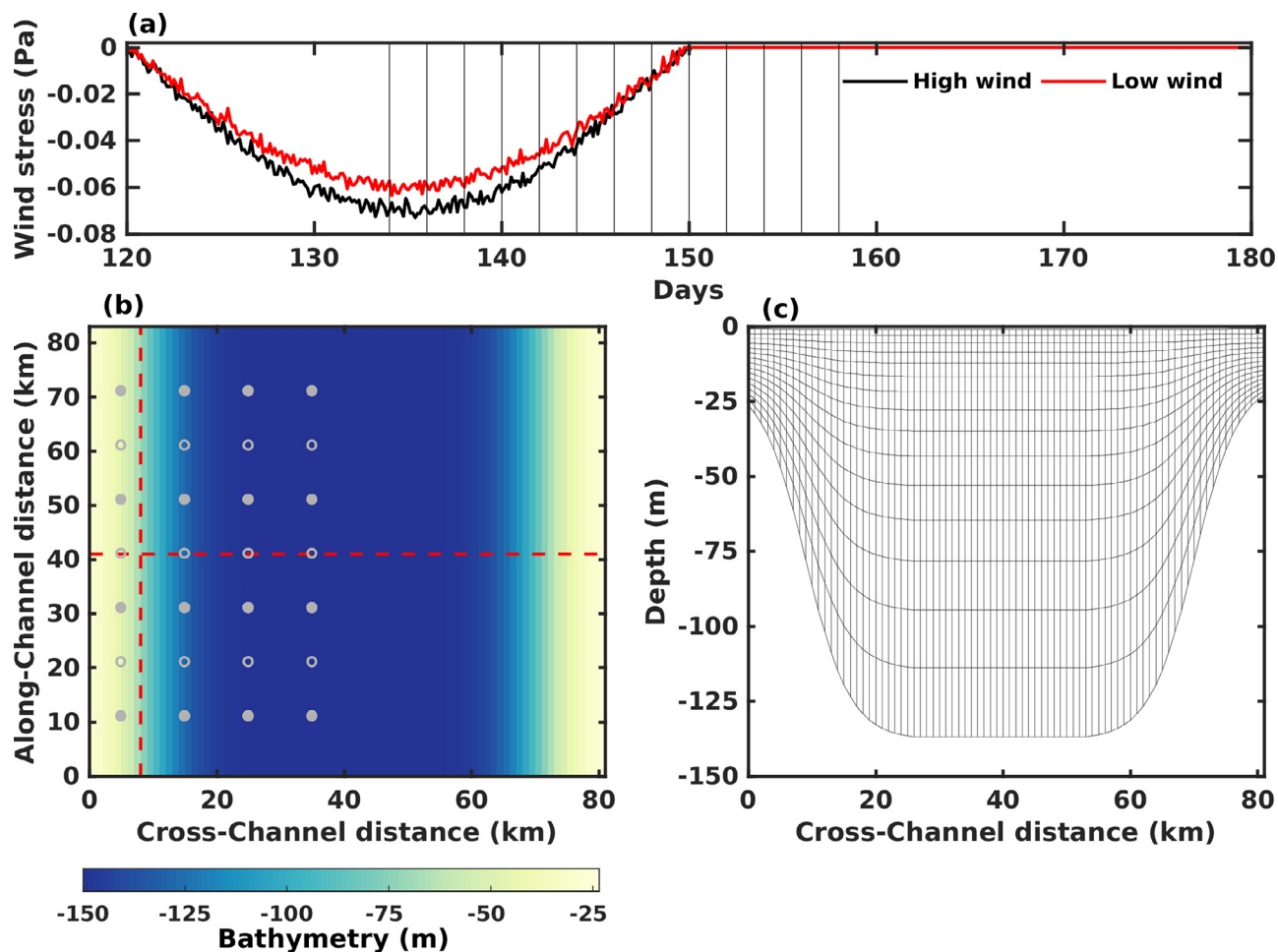


Fig. 1. (a) Wind stress for the high-wind and low-wind model runs. The vertical lines indicate the timing of assimilation steps. (b) Model bathymetry and (c) vertical grid of cross-channel transect. The red dashed lines in (b) show the position of the cross-channel transect and an along-channel section. The circles show the 28 stations where temperature profiles are sampled. The filled circles show the 16 stations where nitrate profiles are sampled. (For interpretation of the references to colour in this figure legend, the reader is referred to the web version of this article.)

satellite-derived chlorophyll, into coupled physical–biogeochemical models (e.g., Natvik and Evensen, 2003; Gregg, 2008; Ciavatta et al., 2011; Hu et al., 2012; Ford et al., 2012; Fontana et al., 2013; Ford and Barciela, 2017). Assimilation of satellite ocean color products other than chlorophyll, such as phytoplankton absorption coefficients (Shulman et al., 2013), diffuse light attenuation coefficients (Ciavatta et al., 2014), and remote-sensing reflectance (Jones et al., 2016) are also being pursued. However, it has long been recognized that deficiencies in biogeochemical fields can arise from deficiencies in the physical state (e.g., Doney, 1999; Oschlies and Garçon, 1999; Doney et al., 2004) because the physics controls both horizontal and vertical transport of nutrients, oxygen, plankton and many other biogeochemical variables. Several studies have investigated the impact of assimilating physical data alone on coupled physical–biogeochemical systems (Berline et al., 2007; Samuelsen et al., 2009; While et al., 2010; El Moussaoui et al., 2011; Fiechter et al., 2011; Raghukumar et al., 2015). One important and perhaps surprising finding drawn from these studies is that, despite the clear improvement in physical model fields, the physical data assimilation alone does not generally improve, but often degrades, simulated biogeochemical fields. For example, While et al. (2010) and El Moussaoui et al. (2011) reported overestimated surface nutrients and chlorophyll concentrations, particularly in equatorial regions, associated with spurious increases in vertical velocities when assimilating physical data in global ocean models. Berline et al. (2007) found large increases in vertical nutrient fluxes in mid-latitudes and sub-tropics that were partly due to the misalignment

between physical and biogeochemical fields resulting from updates of the physical fields. Raghukumar et al. (2015) also showed that assimilating physical data leads to elevated production, particularly in oligotrophic regions, and attributed the overestimation to a net upward nutrient flux resulting from high vertical velocity fluctuations due to the “initialization shocks” after updates to the density distribution, and increased nutrient variance on density surfaces due to the adjustment of physical variables in the assimilation step.

Collectively the above studies demonstrate that adjusting only physical or biogeochemical fields is not sufficient to improve the full 3D biogeochemical model state. An obvious next step is the simultaneous updating of physical and biogeochemical fields. Two approaches have emerged to address it. The simpler approach is applying a correction to the nutrient field alongside the physical data assimilation (Shulman et al., 2013; While et al., 2010). The second approach is to jointly assimilate physical and biogeochemical observations into the models. To date, few studies have explored this idea but with encouraging results (Anderson et al., 2000; Ourmières et al., 2009; Song et al., 2016a,b; Mattern et al., 2016). These studies show that assimilating both physical and biogeochemical data can maintain dynamical consistency between the physical and biogeochemical fields and provide better state estimates than only assimilating one or the other. However, one clear drawback of this approach is that the required physical and biogeochemical observations might not always be available concurrently.

Here we propose and test an alternative approach for updating both

types of model fields even when only one data type (biogeochemical or physical) is available. The approach takes advantage of the inherently multivariate nature of the Ensemble Kalman Filter (EnKF) to generate multivariate increments that can be applied consistently to all model state variables. While the EnKF has been used to assimilate physical or biological ocean observations in the past, its ability to update biological model fields by assimilating physical observations and *vice versa* has not yet been tested in ocean applications. This paper aims to systematically assess whether, when and why multivariate EnKF updates of both physical and biogeochemical fields can outperform isolated updates of physical or biogeochemical fields by assimilating only one observation type, and compare these two DA strategies against the joint updates of both fields by assimilating both observation types. This is achieved by conducting a series of twin experiments in an idealized ocean channel that experiences wind-driven upwelling.

2. Model description and experimental setup

2.1. The coupled physical–biogeochemical model

We use the Regional Ocean Modeling System (Haidvogel et al., 2008; ROMS, <http://myroms.org>), configured in a computationally efficient idealized channel. ROMS is a free-surface, terrain-following, primitive equation ocean model that has been used extensively for coupled physical–biogeochemical modeling and data assimilation (e.g., Hu et al., 2012; Raghukumar et al., 2015; Song et al., 2016a,b). The idealized channel is 82 km wide, with the depth symmetrically increasing from 25 m at the two edges to 140 m in the middle (Fig. 1). The model grid is uniformly spaced with a horizontal resolution of 1 km, generating 84 cross-channel and 82 along-channel grid points, and has 16 terrain-following vertical layers with thickness ranging from 1.6 m at the surface near the channel edges to 22.6 m at the bottom of the mid-channel. Periodic lateral boundary conditions are applied to the southern and northern open boundaries; that is, any physical or biogeochemical tracer or flow that leaves the domain through one boundary will re-enter at the opposite side. Vertical mixing is parameterized using the Mellor and Yamada (1982) Level 2.5 turbulence closure scheme. Bottom friction is specified using a linear drag formulation.

The model is forced with a uniform along-channel wind that generates upwelling on one side of the channel and downwelling on the other. The wind forcing is prescribed by a clipped sine curve resulting in 30 days of non-zero wind stress followed by 30 days of relaxation without any wind forcing. Gaussian noise with a standard deviation of 0.002 Pa is added to generate a more realistic wind regime. One cycle with a peak wind stress of 0.07 Pa (high wind) and 0.06 Pa (low wind) is shown in Fig. 1a.

The biogeochemical component of the coupled model uses the nitrogen cycle model of Fennel et al. (2006). The model is a relatively simple representation of the pelagic nitrogen (N) cycle, including two species of dissolved inorganic nitrogen, nitrate (NO₃) and ammonium (NH₄); one phytoplankton group (Phy); chlorophyll (Chl) as a separate state variable to allow for photoacclimation; one zooplankton group (Zoo); and two pools of detritus representing large, fast-sinking particles (LDet) and suspended, small particles (SDet). The model accounts for photoacclimation of phytoplankton based on the model of Geider et al. (1997), resulting in a variable ratio of chlorophyll to phytoplankton biomass. In the model, the biogeochemical fields do not influence physical fields, i.e. there is no feedback from biology to physics. This coupled model has been a valuable tool for understanding interacting physical and biogeochemical processes within realistic configurations for both coastal (e.g., Fennel et al., 2006, 2008) and open ocean ecosystems (e.g., Xue et al., 2013), as well as for data assimilation experiments (e.g., Hu et al., 2012; Mattern et al., 2013).

The biogeochemical component of the coupled model was spun up for 1 year without any wind forcing, and no flow at the lateral

boundaries. The initial temperature ranges from 14.5 °C at the mid-channel bottom to 22 °C at the surface, initial nitrate ranges from 13.5 mmol N m⁻³ at depth to 0.5 mmol N m⁻³ at the surface, and all other initial biogeochemical variables were homogeneous at a low positive value. Salinity was fixed at 35 PSU and surface heat flux was not included in this idealized setup. The biogeochemical variables reached a steady state after 1 year of spin-up. The spun-up biogeochemical fields were used as initial condition for all coupled simulations, which were forced with high or low wind (Fig. 1a) for 180 days (covering three wind cycles).

2.2. Experimental framework

The performance of different data assimilation strategies is evaluated in twin experiments that consist of a reference model run representing the ‘truth’ from which synthetic observations are generated, and a model with biased physics and biology that is subject to ensemble-based assimilation of the synthetic observations. We test two contrasting scenarios: Scenario 1, where the forecast model is forced with lower wind stress and a lower photosynthesis-irradiance (PI) parameter value than the truth leading to underestimation of the true upwelling and productivity; Scenario 2, where a higher wind stress and higher PI value lead to overestimation of upwelling and productivity. For the sake of brevity, we only detail the experimental setup of Scenario 1; Scenario 2 is identical except for the wind forcing and biological parameter set.

In Scenario 1, the reference (or ‘truth’) is generated by running the coupled model as described in Section 2.1. and forced with higher wind (peak wind stress of 0.07 Pa, denoted as high wind in Fig. 1a). The along-channel, northward wind leads to upwelling of nutrient-rich, cold water at the western edge of the channel stimulating phytoplankton growth (assuming Coriolis frequency $f > 0$).

Synthetic observations are sampled from the reference run, including sea surface height (SSH), sea surface temperature (SST) and surface chlorophyll at all grid points (assuming no data missing due to cloud cover), and 28 temperature and 16 nitrate profiles from a regular sampling grid (see Fig. 1b). Typical Gaussian observation errors of $N(0, 0.3\text{ °C})$ for temperature (both SST and temperature profiles), $N(0, 1\text{ cm})$ for SSH, $N(0, 35\% \cdot \text{true concentration})$ for surface chlorophyll, and $N(0, 10\% \cdot \text{true concentration})$ for nitrate profiles are added to the synthetic data. In addition, smaller errors in the biological observations, i.e. $N(0, 10\% \cdot \text{true concentration})$ for chlorophyll and $N(0, 5\% \cdot \text{true concentration})$ for nitrate, are tested as described in Section 2.2.3.

In the biased model, the peak wind stress is about 14% smaller. Gaussian noise with a standard deviation of 0.002 Pa was added to the wind stress to create an ensemble of wind forcing files (one realization is shown in Fig. 1a, denoted as low wind). In addition, the five biological parameters to which the system is most sensitive were perturbed. These parameters were identified in sensitivity experiments as follows. For each parameter the model was run twice, after doubling and halving the parameter value. The five parameters for which these perturbations resulted in the largest Root Mean Square (RMS) difference to the unperturbed simulation are referred to as the most sensitive ones. In the ensemble simulations, all five parameters are sampled from a uniform distribution around their nominal value with a variance of 75% of the nominal value. The nominal values of the top two most sensitive parameters, the photosynthesis-irradiance initial slope ($0.015\text{ mg C (mg chl W m}^{-2}\text{ d)}^{-1}$) and zooplankton grazing rate (0.6 d^{-1}), are set to be 40% lower than those of the reference run to simulate model bias errors. The other three parameters, phytoplankton growth rate (1.0 d^{-1}), mortality rate (0.1 d^{-1}), and maximum chlorophyll to carbon ratio ($0.0535\text{ mg chl (mg C)}^{-1}$), are not biased.

2.2.1. DEnKF algorithm

We use the deterministic formulation of the EnKF (DEnKF), which was introduced by Sakov and Oke (2008) and has been used previously

in biogeochemical data assimilation applications (e.g., Simon et al., 2015; Jones et al., 2016).

The central idea underlying the EnKF is that an ensemble of model simulations can be used to approximate the model's estimate of uncertainty, and that the model state can be updated using available observations as the ensemble is integrated forward in time (Evensen, 1994). The EnKF algorithm consists of sequential forecast and analysis steps. During the forecast step, the model ensemble is propagated forward in time. During the analysis step, the model state is updated using the Kalman Filter (KF) analysis equation:

$$\mathbf{x}^a = \mathbf{x}^f + \mathbf{K}(\mathbf{d} - \mathbf{H}\mathbf{x}^f), \quad (1)$$

where \mathbf{x} is the $n \times 1$ model state estimate vector (n is the number of model state variables at all grid points), the superscripts a and f represent the analysis and the forecast estimates, respectively, \mathbf{d} is the $m \times 1$ vector of observations (m is the number of available observations), \mathbf{H} (linear in this form, dimension of $m \times n$) is the measurement operator mapping the model state onto the observations, and \mathbf{K} is the $n \times m$ Kalman gain matrix, given as

$$\mathbf{K} = \mathbf{P}^f \mathbf{H}^T (\mathbf{H} \mathbf{P}^f \mathbf{H}^T + \mathbf{R})^{-1} \quad (2)$$

where \mathbf{P}^f represents the $n \times n$ prior sample error covariance matrix (approximated using the forecast ensemble), \mathbf{R} is the $m \times m$ observation error covariance, and superscript T denotes matrix transpose.

In the original stochastic EnKF (Burgers et al., 1998), the forecast ensemble \mathbf{X}^f is updated via Kalman analysis Eq. (1) and requires perturbing observations \mathbf{d} in order to obtain an analysis error covariance consistent with that given by the (linear) Kalman Filter. In contrast, the DEnKF updates the ensemble mean and ensemble anomalies separately without perturbing observations, and is hence termed ‘deterministic’. First, the forecast ensemble mean $\bar{\mathbf{X}}^f$ is updated as in Eq. (1). Then, the forecast ensemble anomalies \mathbf{A}^f are updated by $\mathbf{A}^a = \mathbf{A}^f - \frac{1}{2} \mathbf{K} \mathbf{H} \mathbf{A}^f$, which ensures that the resulting covariance matrix is slightly inflated compared to the theoretical value given by the Kalman Filter. Finally, the analysis ensemble is reconstructed as $\mathbf{X}^a = \mathbf{A}^a + [\bar{\mathbf{X}}^a, \dots, \bar{\mathbf{X}}^a]$. For more details on the DEnKF see Sakov and Oke (2008).

In principle, the DEnKF can update the entire model state based on the correlations in the ensemble covariance between the observations and model variables. However, computational constraints often prohibit inclusion of all 3D state variables in the assimilation state vector \mathbf{X}_i^f (the i th ensemble member). Here we limit updates to the four biological variables (nitrate, chlorophyll, phytoplankton and zooplankton) and one physical variable (temperature) that are most relevant to the dynamics of the system.

2.2.2. Assimilation settings

We chose an ensemble size of 20 for our data assimilation experiments. Relatively small ensembles like this can lead to spurious correlations between distant grid points. To prevent the potential negative effects of spurious correlations, we applied a distance-based localization method known as local analysis (Evensen, 2003; Hunt et al., 2007; Sakov and Bertino, 2011). In local analysis, the spatial domain of influence of each observation is artificially reduced by multiplying the ensemble anomalies and innovations with a distance-dependent localization function (Gaspari and Cohn, 1999). We chose a localization radius of 20 km for SST, SSH, temperature profiles and nitrate profiles, and 10 km for surface chlorophyll. Additionally, to account for the underestimation of the forecast error covariance due to the small ensemble size, an inflation factor of 1.05 was applied to the ensemble anomalies inflating the ensemble around its mean at every update step (Anderson and Anderson, 1999). The localization radius and inflation factor are based on initial tests that involve selecting the values that best reduce the model-data errors without causing ensemble collapse or generating discontinuities in the analyzed fields.

Additional practical implementation choices were made to make the DEnKF performance more robust as follows. Because chlorophyll and

nitrate concentrations at some grid points can be as low as 10^{-4} mg/m^3 (for chlorophyll) or mmol/m^3 (for nitrate), resulting in extremely low magnitudes of the observation error covariance \mathbf{R} , we set a lower limit of 10^{-2} for the diagonal elements of \mathbf{R} corresponding to chlorophyll and nitrate observations. This is equivalent to artificially increasing the error of very low chlorophyll and nitrate observations. This can be thought of as applying inflation in the observation space, which has already been explored in Anderson (2009). We also inflate the assumed observation error covariance by a factor of 2 when updating the ensemble anomalies while using the original observation error variance for updating the ensemble mean as proposed in Sakov et al. (2012). This is done to produce a weaker update for the ensemble-based state error covariance without changing the ensemble analysis mean, and hence retain a larger ensemble spread. To prevent an initial shock to the system due to large initial updates, we increased the observation error by a factor of 8, 4 and 2 for the first three DA steps, respectively as in Sakov et al. (2012). Finally, a post-processing step was performed at the end of each update step resetting any negative values of temperature and biogeochemical variables to their corresponding forecast values (less than 0.2% of grid cells were affected by this throughout the assimilation period).

2.2.3. Data assimilation experiments

We carried out a series of assimilation experiments for Scenarios 1 and 2 (Table 1) using different strategies for assimilating a single (biogeochemical or physical) or both observational data types: Method 1 “Isolated updates”, where only one of the two data types is used, either physical observations to update physical model fields or biogeochemical observations to update biogeochemical model fields; Method 2 “Multivariate updates | single data type”, where only one data type is used to update both physical and biogeochemical model fields taking advantage of the multivariate covariance structure within the DEnKF; and Method 3 “Joint updates | both data types”, where both data types are assimilated in a two-step update, with physical observations being used first and biogeochemical observations used next. The acronyms for assimilation experiments introduced in Table 1 are in accord with the posterior probability of the model state given the observations (e.g., $p(\text{model} | \text{observation})$). In all experiments, the DEnKF update is performed every two days during upwelling peaks of the second and third wind cycle (day 74 to 98 and 134 to 158, respectively) leading to 26 assimilation steps in total. Detailed analysis of the experiments focuses on the third wind cycle when the largest deviation between the biased ensemble runs and the true state has developed.

The assimilation impact is assessed by comparing the assimilative runs to an ensemble of model simulations with the same model configuration but without any data assimilation. This ensemble run is referred to as the ‘free run’. The model's forecast skill, a metric of how long the model's forecast from the analysis outperforms the free run, is also assessed. For this purpose, we perform 25-day ensemble runs, referred to as ‘forecast runs’, that are initialized from the updated states on day 140 (the 17th DA step) and forced with the same winds as the assimilation runs.

Model-data misfit is quantified by examining the deviations from the truth (model minus truth). For DA runs at assimilation times, when both forecast and analysis exist, the forecast ensemble mean is used for calculating the deviation. We first computed the daily deviations at each grid point during the analysis period (day 134 to 158), and then averaged the deviation or absolute deviation values over space and time to obtain the mean deviation (bias) and the mean absolute deviation (MAD). Symbols $\text{bias}_{\text{surf}}$ and MAD_{surf} represent bias and MAD averaged over the surface layer only, whereas MAD_{all} represents averaging over the entire water column.

3. Results

Below we provide a detailed analysis of Scenario 1 (the case underestimating upwelling and productivity). Results from Scenario 2 (the

Table 1
Overview of assimilation experiments.

	Experiment	Updated 3D fields			Assimilated observations			
		T	NO3	Chl, Phy, Zoo	SSH, SST	T profiles	Surface chl	N profiles
Method 1 “Isolated updates”	B chl		✓	✓			✓	
	B chl _{10%}		✓	✓			✓	
	B chlN		✓	✓			✓	✓
	B chlN _{5%}		✓	✓			✓	✓
	T P _{surf}	✓			✓			
	T P _{all}	✓			✓	✓		
Method 2 “Multivariate updates single data type”	TB chl	✓	✓	✓			✓	
	TB chl _{10%}	✓	✓	✓			✓	
	TB chlN	✓	✓	✓			✓	✓
	TB chlN _{5%}	✓	✓	✓			✓	✓
	TN P _{surf}	✓	✓		✓			
	TN P _{all}	✓	✓		✓	✓		
Method 3 “Joint updates both data types”	T P _{surf} .B chl	✓1	✓2	✓2	✓1		✓2	
	T P _{all} .B chlN	✓1	✓2	✓2	✓1	✓1	✓2	✓2
	TN P _{surf} .B chl	✓1	✓1, 2	✓2	✓1		✓2	
	TN P _{all} .B chlN	✓1	✓1, 2	✓2	✓1	✓1	✓2	✓2

Assimilated or updated fields are checked (✓). The numbers 1 and 2 in Method 3 experiments indicate the step where the corresponding field is assimilated or updated. The second column gives the code for each experiment. In accord with the posterior probability of the model state given the observations (e.g., $p(\text{model} | \text{observation})$) the capital letters that appear before the vertical line define the 3D fields to be updated. B, N and T correspond to the biogeochemical variables (chlorophyll, phytoplankton, zooplankton and nitrate), just nitrate, and temperature, respectively. The variables that appear after the vertical line define the observations that are assimilated, where *chl*, N, P_{surf} and P_{all} denote surface chlorophyll, nitrate profiles, physical variables at the surface (SSH and SST), and physical variables at both surface and depth (SSH, SST and T profiles), respectively. The subscript following *chl* (or N) denotes reductions in the observation error of surface chlorophyll (or nitrate profiles) to 10% (or 5%) instead of the default 35% (10%) used in the other experiments. The underscore in Method 3 codes indicates the separation of the two update steps.

case overestimating upwelling and productivity) are presented in Section 3.4.

3.1. Comparison between truth and free run

Time series of domain-averaged surface temperature, nitrate and phytoplankton from the truth, free run and different DA runs are shown in Fig. 2. Compared to the truth, the free run is overall warmer and has lower surface nitrate and phytoplankton due to weaker upwelling. Fig. 3 shows a snapshot of SSH, surface temperature, nitrate and phytoplankton on day 140. SSH anomalies on both upwelling and downwelling edges are smaller in the free run than the truth. In the free run, the band of cold, nutrient-rich water along the upwelling edge is much narrower than in the truth, and the band of elevated phytoplankton concentrations detached from the coast in the truth is not simulated by the free run. The corresponding vertical distributions of the same variables along a cross-channel transect are shown in Fig. 4. The reference isotherm (represented by the 16 °C isotherm) and reference isopleth of nitrate (represented by the 5 mmol NO₃ m⁻³ isoline) coincide and are deeper in the free run than the truth at the upwelling edge. Along-channel section-averaged temperature and nitrate profiles near the upwelling edge (Fig. 5a, e) show that in the free run temperature is warmer and nitrate concentration lower than the truth in the top 60 m. The differences between the truth and free run are also reflected by the positive bias_{surf} in temperature, negative bias_{surf} in nitrate and phytoplankton as well as the large MAD_{all} in all variables (Fig. 6).

3.2. Impact of assimilation on physical and biogeochemical states

3.2.1. Method 1 “Isolated updates”

First, we assess the assimilation impact when biogeochemical variables are used to update only biogeochemical variables, or physical variables to update only physical variables. Assimilating surface chlorophyll to correct the biogeochemical variables alone (B|chl and

B|chl_{10%}) barely affects the time evolution of surface nitrate and improves surface phytoplankton only when the chlorophyll observation error is reduced to 10% (Fig. 2, second row). The point-to-point comparison metrics confirm that B|chl and B|chl_{10%} slightly reduce bias_{surf} and MAD_{surf} for phytoplankton, but B|chl_{10%} leads to an increase in MAD_{all} for nitrate and phytoplankton (Fig. 6). In B|chlN and B|chlN_{5%}, where nitrate profiles are assimilated in addition to surface chlorophyll, the updates in surface nitrate and phytoplankton are more noticeable than in B|chl, but the ensemble mean is still far from the truth (Fig. 2, third row), and the reference isopleth of nitrate in B|chlN is only slightly lifted up to the truth (Fig. 5f). The metrics in Fig. 6 show that B|chlN improves nitrate with a smaller bias_{surf} and MAD_{all} than B|chl. Reducing the nitrate observation error (B|chlN_{5%}) leads to little further improvement relative to B|chlN.

Assimilating SST and SSH (T|P_{surf}) remarkably improves surface temperature and increases surface nitrate and phytoplankton concentrations toward the truth without directly updating them during analysis steps (Fig. 2, fourth row). However, the phytoplankton peak is delayed and concentrations are overestimated after the peak in upwelling. T|P_{surf} clearly lifts up the reference isotherm and isopleth of nitrate toward the truth (Fig. 5c, g), but degrades the nitrate profile at depths greater than 25 m (Fig. 5g). The comparison metrics show that T|P_{surf} improves SSH, temperature, surface nitrate, and phytoplankton with lower biases and MAD values, but degrades subsurface nitrate with higher MAD_{all} than the free run (Fig. 6). Compared to T|P_{surf}, assimilating additional temperature profiles (T|P_{all}) improves the timing of the phytoplankton peak but overestimates phytoplankton more after peak upwelling (Fig. 2, fifth row). Comparison metrics in Fig. 6 show that T|P_{all} further improves temperature with lower MAD_{all}, but degrades nitrate with higher MAD values than those in T|P_{surf} and the free run (Fig. 6).

None of the Method 1 “Isolated updates” approaches satisfactorily improves the biogeochemical ocean model state, although the physical model state is remarkably improved by assimilating the physical data.

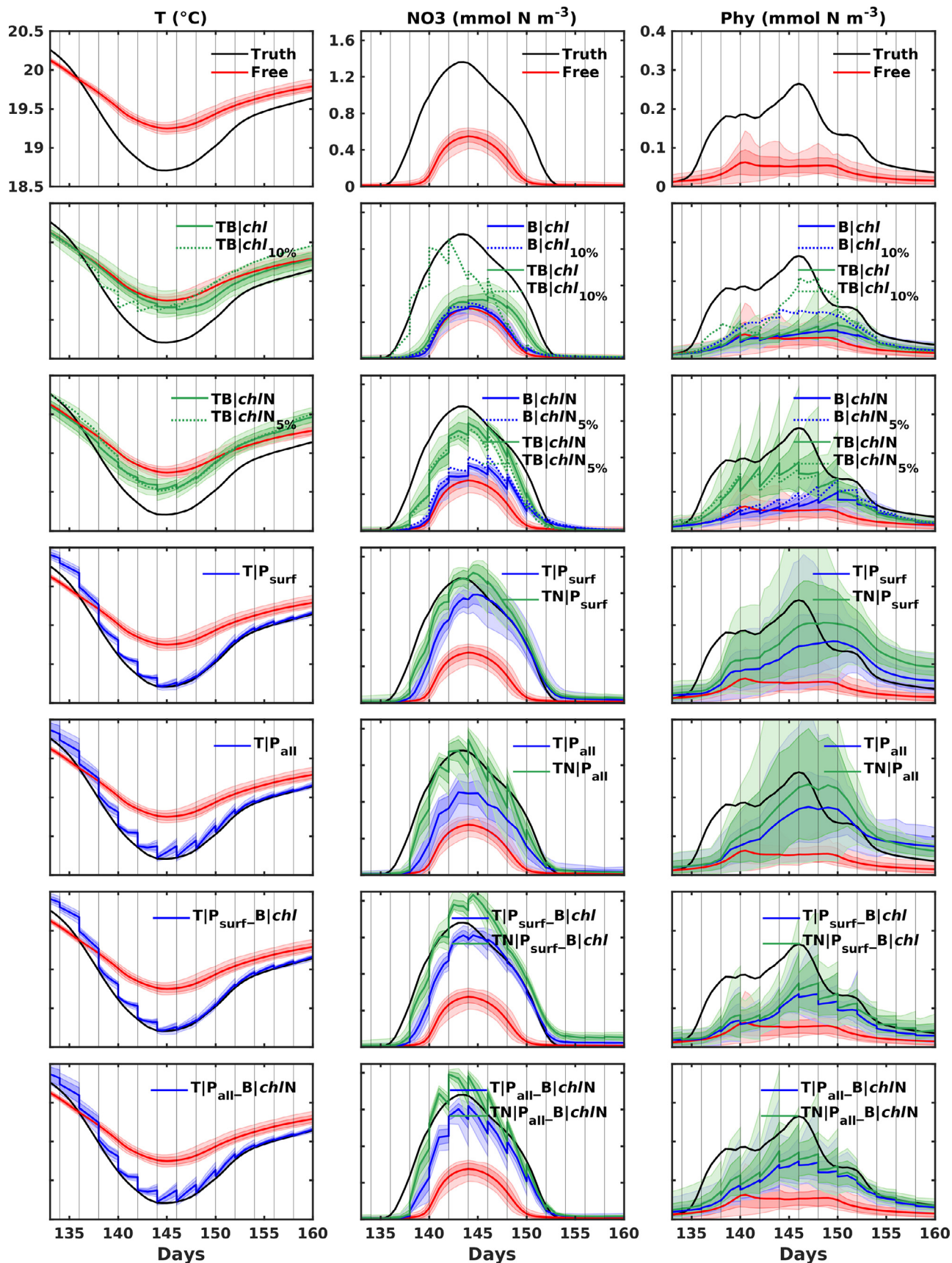


Fig. 2. Time series of the surface domain-averaged water temperature (T), concentrations of nitrate (NO₃), and phytoplankton (Phy) for truth, free run and different assimilation runs. For the free and assimilation runs, the ensemble means are shown as solid colored lines, the standard deviation of the ensemble as dark colored area, and the range between the minimum and maximum value of the ensemble as light colored area. Black vertical lines indicate the timing of assimilation steps. (For interpretation of the references to colour in this figure legend, the reader is referred to the web version of this article.)

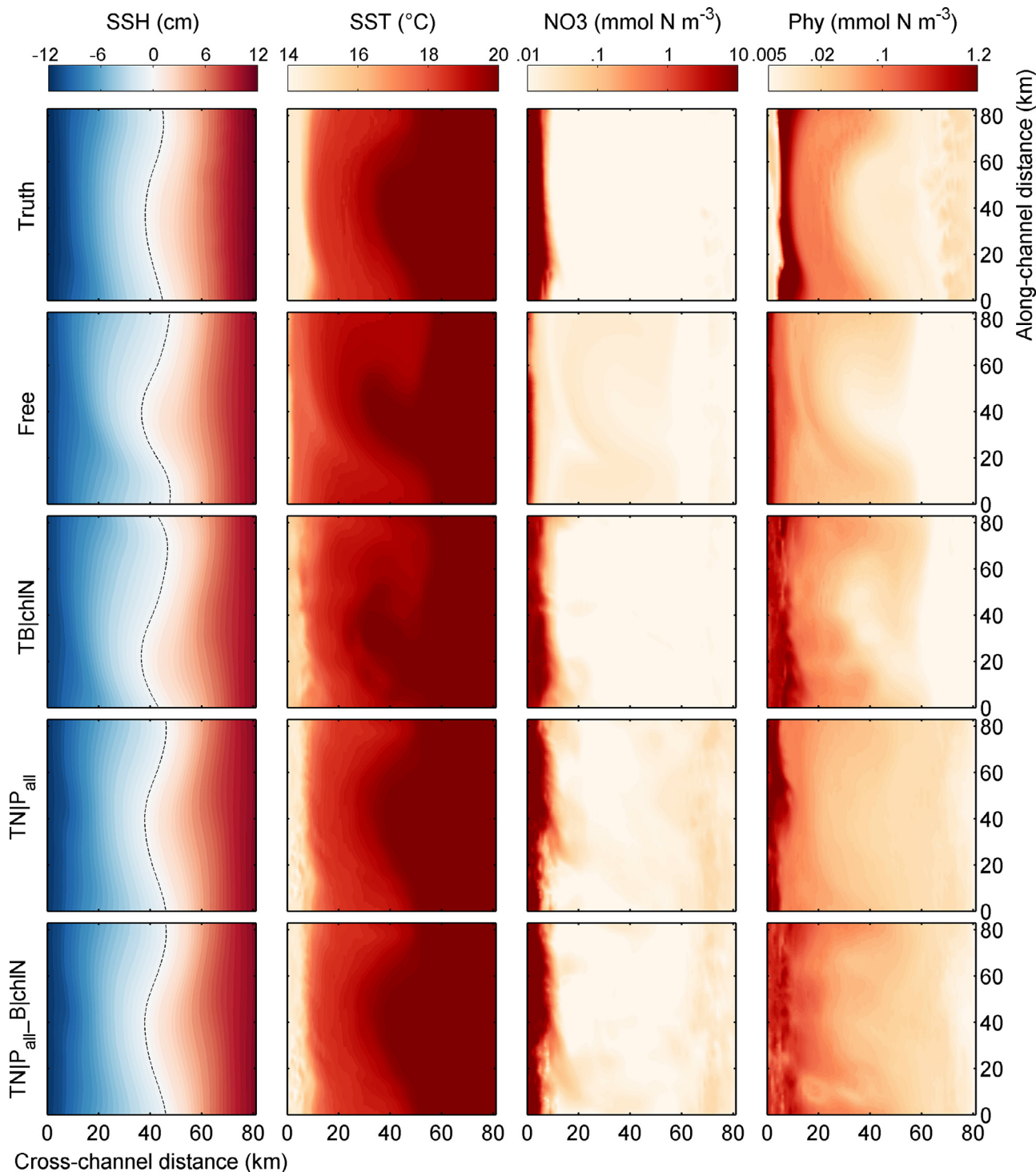


Fig. 3. Surface layer on day 140 (assimilation step 17) for different state variables from the truth, free run and different assimilation runs. The black dashed line shows the zero contour line. (For interpretation of the references to colour in this figure legend, the reader is referred to the web version of this article.)

3.2.2. Method 2 “Multivariate updates | single data type”

Second, we assess the impact of multivariate updates, where a single data type (biogeochemical or physical observations) is used for multivariate updates of biogeochemical variables and temperature. Assimilating only surface chlorophyll (TB|chl) slightly improves surface temperature and nitrate relative to B|chl (Fig. 2, second row) with slightly smaller $bias_{surf}$ and MAD_{all} (Fig. 6). Reducing the chlorophyll observation error (TB|chl_{10%}) leads to larger increases in surface nitrate and phytoplankton (Fig. 2, second row) that further reduce their $bias_{surf}$ and nitrate MAD_{surf} , but also substantially increases nitrate MAD_{all} .

Assimilating additional nitrate profiles to update both physical and biogeochemical fields in TB|chlN and TB|chlN_{5%}, remarkably improves the time evolution of surface temperature during the upwelling period, and nitrate and phytoplankton for the entire time period (Fig. 2, third row) compared to B|chlN, B|chlN_{5%} and TB|chl. Improvement in TB|chlN is also obvious in the spatial distributions, with an extended area of cold and high-nutrient water along the upwelling edge (Fig. 3) and a clear lift of the reference isotherm near the surface and isopleth of nitrate toward the truth compared to the free run and B|chlN (Figs. 4 and 5). TB|chlN and TB|chlN_{5%} yield the smallest MAD_{all} for all

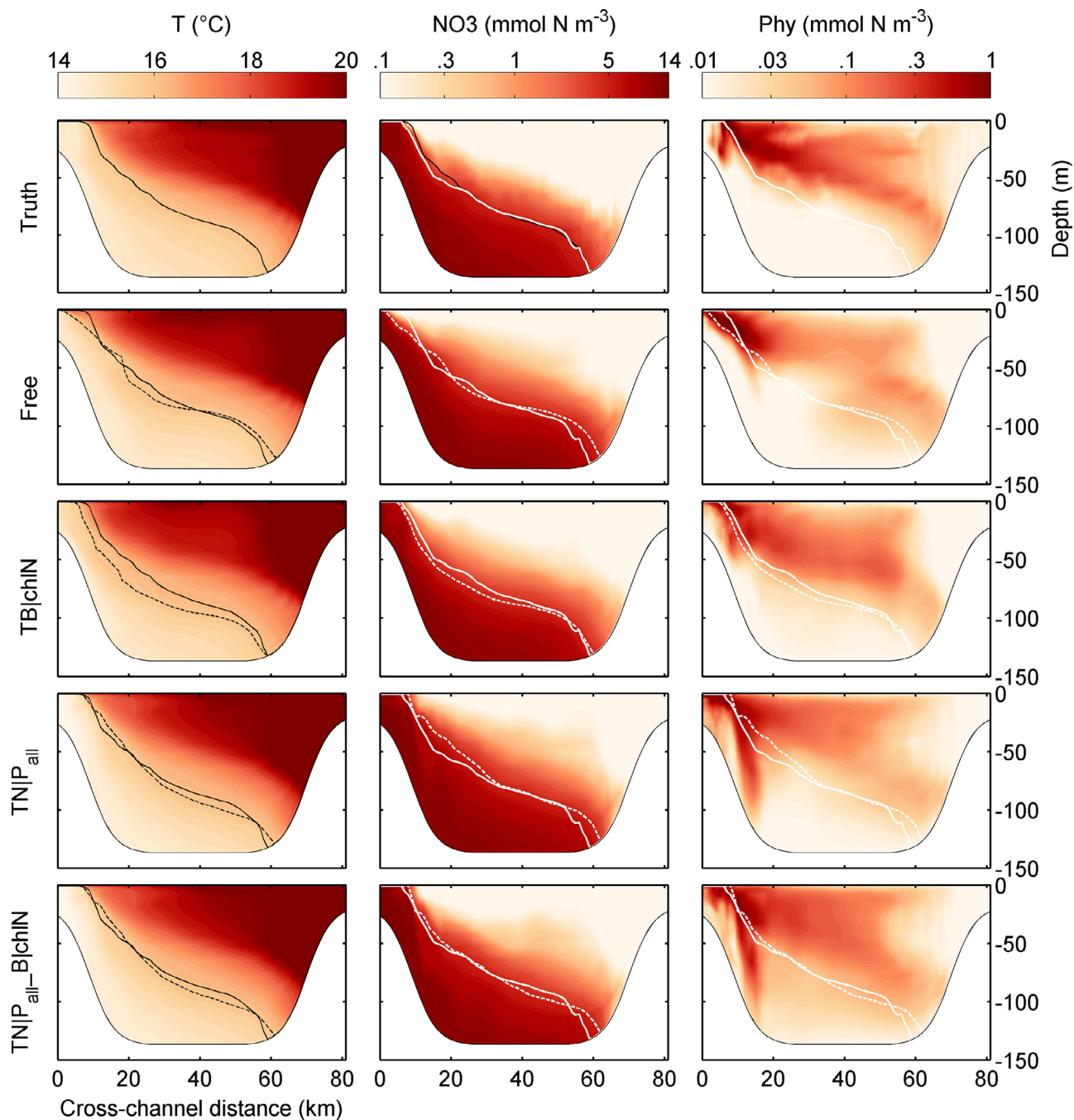


Fig. 4. Cross-channel transect (see Fig. 1 for its location) on day 140 (assimilation step 17) for different state variables from the truth, free run and different assimilation runs. The 16 °C isotherm and 5 mmol $\text{NO}_3 \text{ m}^{-3}$ isopleth for the truth are marked as solid black and white lines, respectively. Dashed black and white lines mark the 16 °C isotherm and 5 mmol $\text{NO}_3 \text{ m}^{-3}$ isopleth for the actual simulation in each panel. (For interpretation of the references to colour in this figure legend, the reader is referred to the web version of this article.)

variables among DA runs that only assimilate biogeochemical observations (Fig. 6).

Then we used physical observations (SSH and SST in $\text{TN|P}_{\text{surf}}$; SSH, SST and temperature profiles in TN|P_{all}) for multivariate updates of physical variables and the nitrate field. We only update the nitrate field instead of all biogeochemical variables because of the high correlation between physical fields and nitrate in contrast to the relatively low correlation between physical fields and other biogeochemical variables. Compared to T|P_{surf} and T|P_{all} (Method 1), $\text{TN|P}_{\text{surf}}$ and TN|P_{all} lead to larger increases in surface nitrate and phytoplankton and overall agree better with the truth except that surface phytoplankton is overestimated after peak upwelling (Fig. 2, fourth and fifth rows). TN|P_{all} also

remarkably improves the spatial distribution of surface and subsurface temperature and nitrate, but fails to improve that for phytoplankton (Figs. 3 and 4). Vertically viewed, both $\text{TN|P}_{\text{surf}}$ and TN|P_{all} effectively lift the depths of reference isotherm and isopleth of nitrate approaching the truth (Fig. 5). Overall TN|P_{all} yields lower MAD_{all} for temperature and nitrate than $\text{TN|P}_{\text{surf}}$ (Fig. 6).

Method 2 “Multivariate updates | single data type” improves the physical and biogeochemical ocean model states more satisfactorily than Method 1 “Isolated updates” does.

3.2.3. Method 3 “Joint updates | both data types”

The last set of assimilation experiments used both data types

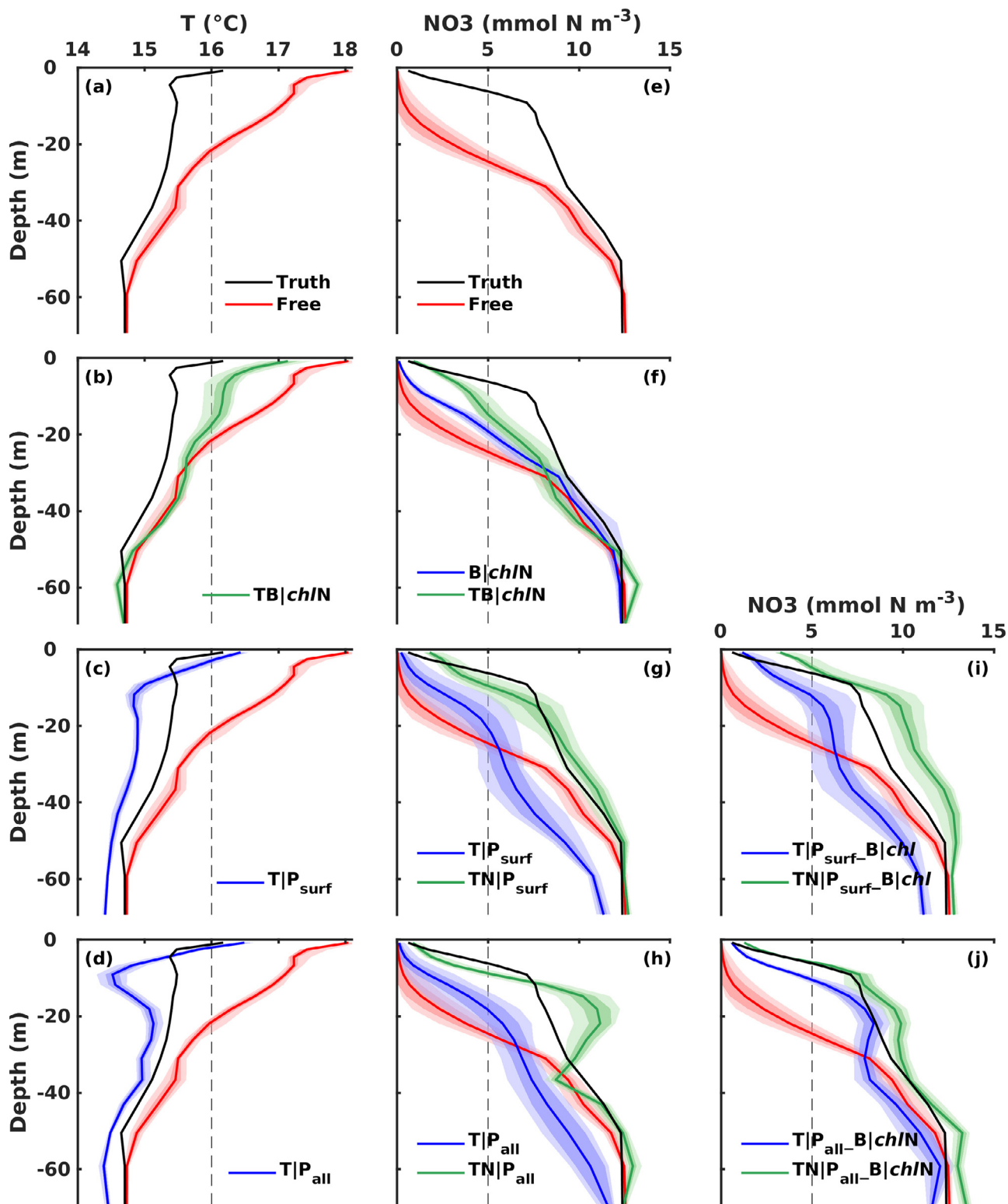


Fig. 5. Averaged (a–d) temperature (T) and (e–j) nitrate (NO₃) profiles over stations along the along-channel section (see Fig. 1 for their locations) on day 140 (assimilation step 17) for the truth, free run and different assimilation runs. For the free and assimilation runs, the solid colored lines represent ensemble means of the section-averaged profiles, the dark colored areas represent standard deviation of the ensemble, and the light colored areas represent range between the minimum and maximum value of the ensemble. The positions of 16 °C isotherm and 5 mmol NO₃ m⁻³ isopleth are marked as dashed lines. (For interpretation of the references to colour in this figure legend, the reader is referred to the web version of this article.)

(physical and biogeochemical observations) to provide a two-step update, where physical observations are assimilated first to update physical fields or both types of fields and biogeochemical observations are assimilated next to update biogeochemical fields only. We have also

performed tests where in the second step biogeochemical observations are used to update both types of variables but found this slightly degraded the updated physical fields from step one, probably because in the first step physical observations already provide sufficient

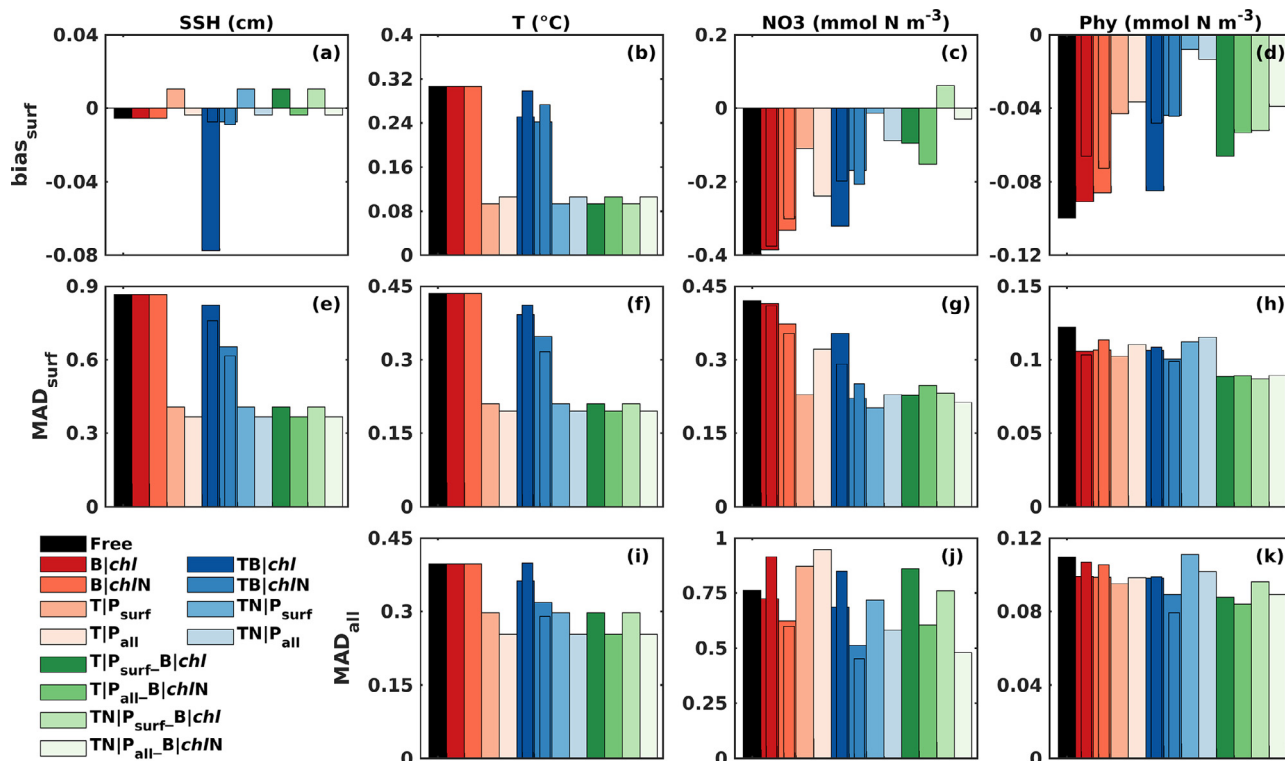


Fig. 6. The domain- and time-averaged (a–d) $\text{bias}_{\text{surf}}$, (e–h) MAD_{surf} and (i–k) MAD_{all} for different state variables from the free run and different assimilation runs. The narrower bars partially overlapping some assimilation runs represent the metrics for sensitivity runs with lower observation error of chlorophyll ($\text{B|chl}_{10\%}$ in dark red and $\text{TB|chl}_{10\%}$ in dark blue) and nitrate ($\text{B|chlN}_{5\%}$ in 2nd red bar and $\text{TB|chlN}_{5\%}$ in 2nd blue bar), respectively. (For interpretation of the references to colour in this figure legend, the reader is referred to the web version of this article.)

improvement to physical fields. Here we used a two-step update approach for two practical reasons: (i) its relatively lower computation cost, and (ii) ease of selecting subsets of variables to be updated. Theoretical considerations do provide some support for the two-step update. Specifically in a Bayesian formulation, if the observations have non-correlated errors, one and two-step updates should produce the same results (e.g., Bierman, 1977). We note however, this exact equivalence is broken by the presence of localization, inflation, and the linearity assumption underlying the EnKF.

Compared with the physical DA runs (T|P_{surf} , T|P_{all} , $\text{TN|P}_{\text{surf}}$ and TN|P_{all}), Method 3 runs ($\text{T|P}_{\text{surf-B|chl}}$, $\text{T|P}_{\text{all-B|chlN}}$, $\text{TN|P}_{\text{surf-B|chl}}$ and $\text{TN|P}_{\text{all-B|chlN}}$) are as effective in increasing the surface nitrate, but underestimate surface phytoplankton slightly more during peak upwelling while agreeing better with the truth afterwards (Fig. 2, sixth and seventh row). Similar to TB|chlN and physical DA runs, Method 3 effectively raises the reference isopleth of nitrate to the truth (Figs. 4 and 5). However, $\text{T|P}_{\text{surf-B|chl}}$ and $\text{TN|P}_{\text{surf-B|chl}}$ lead to relatively high MAD_{all} for nitrate, similar to that in T|P_{surf} and $\text{TN|P}_{\text{surf}}$, suggesting that the assimilation of additional surface chlorophyll has little information to constrain subsurface nitrate. With additional profile observations, $\text{T|P}_{\text{all-B|chlN}}$ and $\text{TN|P}_{\text{all-B|chlN}}$ simulate nitrate profiles that better delineate the true pattern throughout the water column (Fig. 5i, j) and substantially reduce MAD_{all} for nitrate than $\text{T|P}_{\text{surf-B|chl}}$ and $\text{TN|P}_{\text{surf-B|chl}}$ (Fig. 6).

Among all DA runs across different methods (with the same observation error applied), $\text{TN|P}_{\text{all-B|chlN}}$ generally yields the lowest MAD_{surf} or MAD_{all} for all variables presented in Fig. 6 as well as zooplankton, small and large detritus listed in Table 2. Based on Table 2, the Method 2 and Method 3 generally yield beneficial effects on more biogeochemical variables than Method 1. Interestingly, despite the beneficial effects on phytoplankton in many assimilation runs, zooplankton is barely improved except in $\text{TN|P}_{\text{all-B|chlN}}$ and $\text{TB|chlN}_{5\%}$.

We found that surface zooplankton is persistently underestimated in all assimilation runs (not shown), consistent with the lower grazing rate used in the biased model in Scenario 1. Also noticeable from Table 2 is that small and large detritus are improved in all assimilation runs except those only assimilating surface chlorophyll, while ammonium is least improved by assimilation among all variables.

3.2.4. Nitrate and temperature correlation

To investigate whether and to what degree the assimilation affects the correlation between temperature and nutrients, we present scatterplots of nitrate and temperature from the 28 stations shown in Fig. 1b at all assimilation dates (Fig. 7). In the free run (Fig. 7a), there is a tight correlation between temperature and nitrate in nitrate-rich subsurface water, the variance of the nitrate concentration around the best fit between nitrate and temperature is small and its PDF (probability density function) peaks sharply near 0 (Fig. 7h). Compared to the free run, Method 1 runs that adjust only the nitrate or temperature fields (B|chlN in Fig. 7b and T|P_{all} in Fig. 7c) and a Method 3 run that has weak effect on nitrate with assimilation of surface chlorophyll ($\text{T|P}_{\text{surf-B|chl}}$ in Fig. 7d) degrade the temperature–nitrate relationship. In these cases the nitrate variance on temperature surfaces increases by more than 4 times and flatter, more skewed PDFs of nitrate result (Fig. 7h, i, j) compared to the free run. In contrast, assimilation runs in which temperature and nitrate are adjusted simultaneously either based on multivariate updates (Method 2 runs TB|chlN in Fig. 7e and TN|P_{all} in Fig. 7f, and Method 3 run $\text{TN|P}_{\text{surf-B|chl}}$ in Fig. 7g) or by assimilating both fields (Method 3 runs $\text{T|P}_{\text{all-B|chlN}}$ and $\text{TN|P}_{\text{all-B|chlN}}$, not shown) better preserve the temperature–nitrate relationship. In these multivariate update runs the nitrate variance increases much less (compared Fig. 7e, f, g with Fig. 7b, c, d) and the PDF of nitrate is much sharper than in isolated update runs (Fig. 7h, i, j).

Table 2
Overview of assimilation effect on physical and biogeochemical model state variables in Scenario 1.

Unit: %	Experiment	SSH	T	NO3	Chl	Phy	Zoo	SDet	LDet	NH4
Method 1	B chl			−4.9	−3.3	−9.7	−2.4	−7.0	−4.2	−3.8
	B chl _{10%}			+20	+13	−2.6	+14	+1.4	+15	+4.6
	B chlN			−18	−2.1	−10	−4.2	−13	−8.7	−8.3
	B chlN _{5%}			−22	+3.7	−3.9	−6.8	−14	−9.0	−9.9
	T P _{surf}	−53	−25	+14	+5.0	−13	−4.9	−32	−20	+4.3
	T P _{all}	−58	−36	+24	+8.6	−10	−3.9	−29	−20	+5.7
Method 2	TB chl	−4.9	−9.0	−10	−6.3	−10	−4.2	−8.1	−6.2	−5.1
	TB chl _{10%}	−12	+0.3	+11	−0.4	−9.8	−1.7	−8.5	−11	−5.8
	TB chlN	−25	−20	−33	−15	−19	−4.8	−23	−15	−5.4
	TB chlN _{5%}	−29	−27	−41	−23	−28	−17	−32	−26	−11
	TN P _{surf}	−53	−25	−5.8	+18	+1.2	−4.9	−32	−19	+4.0
	TN P _{all}	−58	−36	−24	+9.1	−7.2	−2.9	−28	−22	+5.7
Method 3	T P _{surf} _B chl	−53	−25	+13	−6.3	−20	−4.9	−32	−20	+4.2
	T P _{all} _B chlN	−58	−36	−21	−16	−23	−6.6	−33	−23	+4.4
	TN P _{surf} _B chl	−53	−25	−0.2	−1.0	−12	−3.0	−31	−20	+4.5
	TN P _{all} _B chlN	−58	−36	−37	−13	−18	−11	−34	−31	+2.9

The assimilation effect for each variable is quantified by the percentage change of MAD_{all} in each assimilation experiment relative to the Free run MAD_{all}. A decrease larger than or equal to 10% is considered a “beneficial” effect (highlighted in bold), an increase larger than or equal to 10% is considered “detrimental” (highlighted in bold and italic), while less than 10% change is considered “neutral”. Variables that are not affected by assimilation in a specific experiment are left blank.

3.3. Impact of assimilation on the forecast skill

The comparisons of assimilation experiments in previous sections show that Method 2 “Multivariate updates | single data type” and Method 3 “Joint updates | both data types” improve ocean model fields more significantly and better preserve the temperature–nitrate correlation than Method 1 “Isolated updates”. Here we examine whether the different assimilation methods improve model forecast skill and how they differ.

Fig. 8 shows the difference of domain-averaged MAD_{surf} and MAD_{all} between the free and forecast runs for SSH, temperature, nitrate and phytoplankton, where a positive value indicates improvement by assimilation. It is evident that all assimilation methods improve model forecast skill in all or at least some model fields and display positive MAD differences for 10 to 25 days depending on the method and model field. Specifically for physical fields, Method 2 run TB|chlN improves forecast skill of SSH for 24 days and temperature fields for 15 days, which is as good as the physical DA runs (T|P_{all} and TN|P_{all}) and Method 3 runs (Fig. 8a, b, e). Assimilating additional temperature profiles slightly improves forecast skill for physical fields with overall higher MAD differences (e.g., compare T|P_{all}_B|chlN and T|P_{surf}_B|chl in Fig. 8a, b, e). With respect to nitrate, Method 2 (TB|chlN, TN|P_{all}) and Method 3 (all except T|P_{surf}_B|chl, which has little improvement on nitrate MAD_{all}) strongly improve forecast skill for 10 days in surface waters and 12 days in the entire water column. By comparison, Method 1 leads to smaller and shorter-lasting improvements (B|chlN) or even has a deleterious impact (T|P_{all} in nitrate). Assimilating additional profiles brings extra improvement in forecast skill for nitrate (e.g., compare TN|P_{all}_B|chlN and TN|P_{surf}_B|chl in Fig. 8f). For the phytoplankton field, the improvement in forecast skill from assimilation is sustained for longer, with positive MAD_{surf} and MAD_{all} difference for 25 days in all forecast runs except for surface phytoplankton in TN|P_{all}, and overall larger MAD difference in Method 3 runs than Method 2 or Method 1 runs (Fig. 8d, g).

3.4. Sensitivity of the assimilation methods to twin experimental design

We have shown in the above sections that assimilation corrects the “underestimating upwelling and productivity” Scenario 1 by increasing the upwelling and/or concentrations of biogeochemical variables, with the improvements varying among different assimilation methods. The

conclusions drawn in Scenario 1 hold in the contrasting Scenario 2 where upwelling and productivity are overestimated. Consistent with Scenario 1, Fig. 9 shows that when only assimilating surface chlorophyll, Method 2 run TB|chl only slightly outperforms Method 1 run B|chl with slightly reduced upwelling of cold water and nitrate to the surface. However, when additional nitrate profiles are assimilated, the improvement by Method 2 run TB|chlN over Method 1 run B|chlN is clear with both, surface temperature and nitrate, substantially improved. Assimilating physical observations satisfactorily improves surface temperature and results in a better representation of surface nitrate when nitrate is updated along with temperature (TN|P_{all} compared with T|P_{all}). However, both runs, particularly T|P_{all}, substantially increase surface phytoplankton, leading to even larger overestimation of surface phytoplankton than in the free run (Fig. 9). The elevated production at the surface is partially associated with spurious fluctuations in vertical velocity when physical fields are significantly adjusted (e.g., see higher Root Mean Square (RMS) vertical velocity in TB|chlN, TN|P_{surf} and TN|P_{all} in Fig. S1 in the Supplement). As a result, more nutrients are brought from the subsurface to the surface. The problem of overestimating surface phytoplankton is substantially mitigated when surface chlorophyll and nitrate profiles are assimilated in addition to physical observations in TN|P_{all}_B|chlN (Fig. 9).

The quantitative effects are summarized in Table S1 in the Supplement. Compared to Scenario 1, the beneficial effects on biogeochemical variables in Scenario 2, in terms of MAD_{all} reduction, are weaker, but the degradation of biogeochemical fields (except surface nitrate) when assimilating physical observations to update physical fields alone (T|P_{all}) is clearer. Consistent with Scenario 1, Table S1 shows that Method 2 outperforms Method 1 also in Scenario 2 with lower MAD_{surf} and MAD_{all} for all biogeochemical variables. Overall, Method 3 yields the lowest MAD_{surf} or MAD_{all} for physical and biogeochemical variables.

4. Discussion

We have performed a series of twin experiments comparing different assimilation strategies in an idealized upwelling channel that is subject to biased physics, i.e. with weaker or stronger upwelling than the truth, and biased biology, i.e. with perturbed biogeochemical parameters. Our results show that updating the biogeochemical or physical model state alone (Method 1 “Isolated updates”) is not

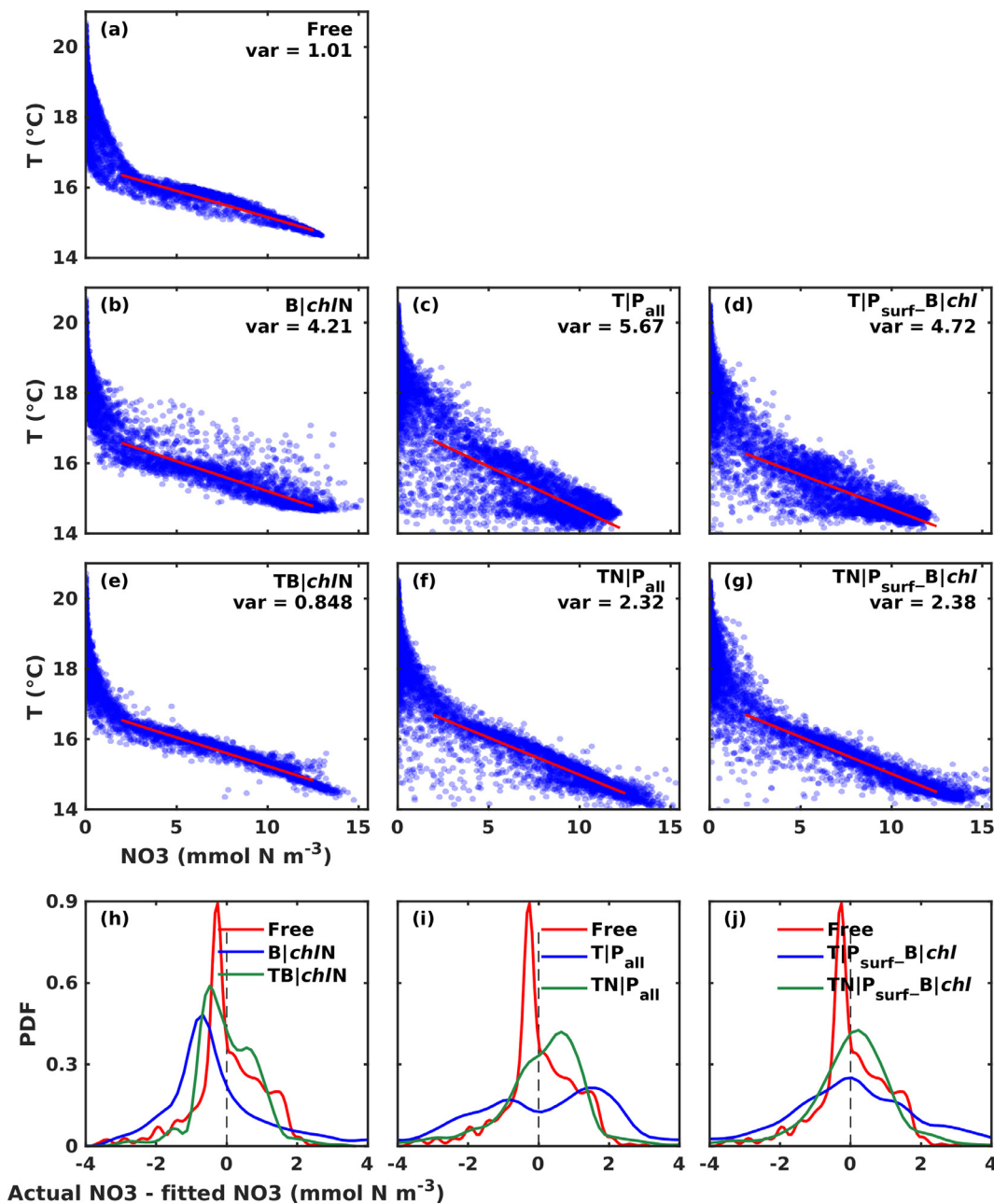


Fig. 7. (a–g) Scatterplots of nitrate (NO_3) and temperature (T) collected from 28 stations shown in Fig. 1b at all depths and at all analysis dates for the free run and different assimilation runs. The red line indicates the linear fit between nitrate and temperature for nitrate concentration between 2 and 12.5 mmol m^{-3} . Variance (var) is calculated as the squared deviation of actual nitrate values from the linear fitted nitrate values at corresponding temperatures. (h–j) Probability density function (PDF) of the deviation of actual nitrate values from fitted nitrate values for each run. (For interpretation of the references to colour in this figure legend, the reader is referred to the web version of this article.)

sufficient for improving the biogeochemical ocean state and forecasts. Without addressing the issue of biased upwelling, which is at the root of the inaccurate simulation of biogeochemical fields, any corrections to the biogeochemical fields during assimilation updates dissipate quickly and do not lead to sustained improvements. When adjusting the physical model state alone, subsurface nitrate distributions are degraded and surface productivity is overestimated despite substantial improvements in physical fields. The degradation in biogeochemical fields is primarily due to two issues: the increased nutrient variance on temperature isosurfaces when only adjusting the temperature or nutrient field, and the spurious, high vertical velocities when physical fields are substantially adjusted. Both issues can result in unreasonable nutrient inputs to the euphotic zone as has been reported in

Raghukumar et al. (2015).

Our experiments show that simultaneously adjusting physical and biogeochemical fields is key to avoid breaking the temperature–nutrient relationship, and to improve the biogeochemical ocean model state estimation. The simultaneous update can be achieved by Method 2 “Multivariate updates | single data type”, which takes advantage of the correlation between physical and biogeochemical fields and the multivariate nature of the Kalman Filter, or by Method 3 “Joint updates | both data types”, which assimilates physical and biogeochemical observations sequentially. In realistic applications, Method 3 is more cumbersome because physical and biogeochemical observations may not be available concurrently. This makes the remarkable improvement obtained by Method 2 very attractive when only one type of

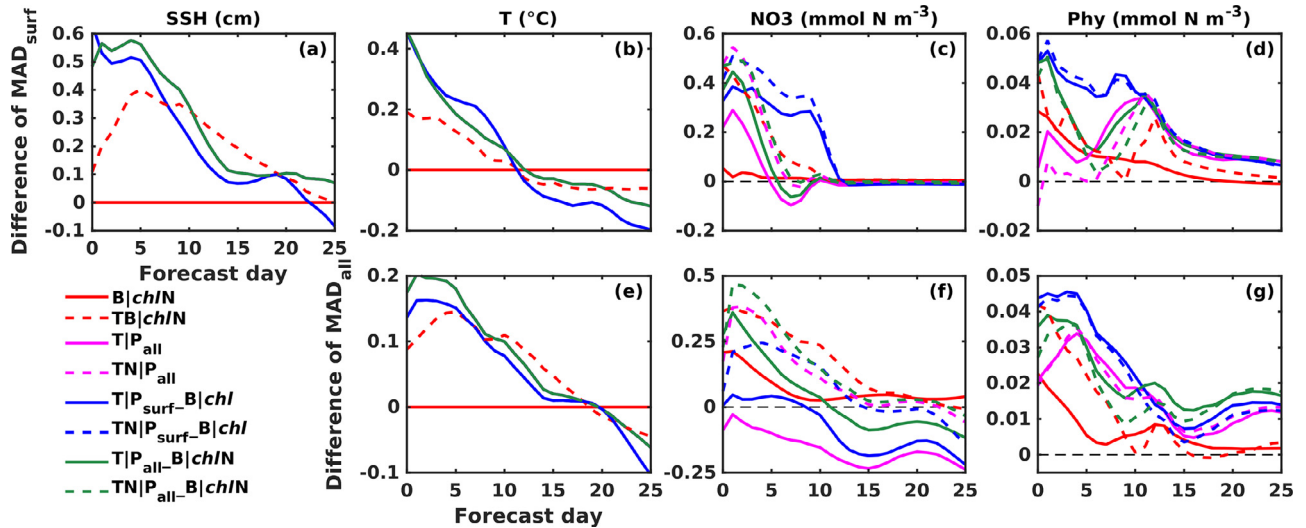


Fig. 8. Difference of domain-averaged (a–d) MAD_{surf} and (e–g) MAD_{all} between the free run and forecast runs initialized from the ensemble analysis on day 140 (assimilation step 17). (For interpretation of the references to colour in this figure legend, the reader is referred to the web version of this article.)

observations is available. In our case, the extra benefit of Method 2 over Method 1 results from a strong correlation between the biogeochemical (or physical) observations and the unobserved physical (or biogeochemical) model fields to be updated, specifically temperature and nitrate. For example, assimilating surface chlorophyll alone leads to limited improvement on the 3D biogeochemical state estimation even when correcting both physical and biogeochemical fields, because the correlation between surface chlorophyll and interior temperature and nitrate fields is weak. This is also confirmed by our sensitivity tests which show that assimilating surface chlorophyll with lower observation error increases the MAD_{all} for temperature and nitrate despite the improvement in surface phytoplankton. In contrast, when additional nitrate profiles are assimilated, the biogeochemical state is much improved and the superiority of Method 2 over Method 1 is much clearer. Reducing the observation error of nitrate profiles further reduces MAD_{all} for all physical and biogeochemical model fields (compare $TB|chlN$ and $TB|chlN_{5\%}$ in Table 2).

Other studies have reported similar success in taking advantage of the relationship between temperature (or density) and nutrients using methods other than EnKF. While et al. (2010) showed that applying an increment to the nutrient field based on the nutrient-potential density relationship during the physical data assimilation improves nutrient distribution. Shulman et al. (2013) found that instantaneously updating nitrate based on observation-derived statistical relations between temperature and nitrate improves model nitrate fields.

Coupled physical–biogeochemical data assimilation as in Method 3 “Joint updates | both data types” has demonstrated success in a few studies using methods other than EnKF (Anderson et al., 2000; Ourmières et al., 2009; Song et al., 2016a, 2016b; Mattern et al., 2016). Here we demonstrate the advantages of Method 3 for the EnKF. Our results add that even when physical and biogeochemical observations are assimilated using Method 3, updating physical and biogeochemical fields simultaneously with physical observations can result in a bigger improvement in the biogeochemical model state (e.g., see higher forecast skills in $TN|P_{surf_B|chl}$ and $TN|P_{all_B|chlN}$ in relative to $T|P_{surf_B|chl}$ and $T|P_{all_B|chlN}$ in Fig. 8c, f). This is especially true when the available biogeochemical observations are not able to effectively constrain the biased biogeochemical fields, i.e. $T|P_{surf_B|chl}$ (where only surface chlorophyll is assimilated to update the biology) fails to reduce the increased nitrate variance on temperature surfaces following assimilation of physical data.

We notice that despite the remarkable improvement in nitrate in Methods 2 and 3 runs which assimilate nitrate profiles ($TB|chlN$ and

$T|P_{all_B|chlN}$), discrepancies between the domain-averaged surface phytoplankton (Figs. 2 and 9) in the DA runs and the truth remain. We attribute these discrepancies to a combination of two factors. First, the relatively high observation error of 35% for chlorophyll results in more modest DEnKF updates than a smaller observation error would. An uncertainty of 35% is typically used for satellite chlorophyll and has been adopted in several prior assimilation studies (e.g., Ciavatta et al., 2011; Hu et al., 2012). Our sensitivity experiments show that reducing the chlorophyll observation error could drive surface phytoplankton closer to the truth (e.g., compared $B|chl_{10\%}$ with $B|chl$, and $TB|chl_{10\%}$ with $TB|chl$ in Fig. 2). Second, we forced the ensemble of free and DA runs with phytoplankton initial slopes and zooplankton grazing rate values that are 40% lower than those for the truth in Scenario 1 and 40% higher in Scenario 2, which act to exacerbate the underestimation or overestimation of productivity. The two factors contributing to the bias in phytoplankton estimation, in addition to the biased physical fields, can also explain the inaccurate zooplankton which is consistently underestimated in Scenario 1 and overestimated in Scenario 2. Improvements could be achieved by applying bias correction methods such as state augmentation to simultaneously estimate and correct biased parameters with the model state variables (e.g., see review in Dee, 2005, and more recent biogeochemical ocean model applications in Simon et al., 2015 and Gharamti et al., 2017a,b) and will be the focus of future work.

We would also like to note that in our experiments, assimilating SSH and SST alone (e.g., $TN|P_{surf}$) is almost as effective as assimilating additional temperature profiles (e.g., $TN|P_{all}$) in lifting the depths of the reference isotherm and isopleth of nitrate toward the truth, primarily due to the tight correlation between SSH and model interior density and nutrient structures (Wilson and Adamec, 2002). It should be noted, however, that surface heat flux was not included in our model simulations. We expect that the performance of assimilating SST to update the thermocline will diminish as surface heat fluxes modify upper water temperatures. Nevertheless, $TN|P_{all}$ outperforms $TN|P_{surf}$ with clearly lower MAD_{all} for temperature, nitrate and phytoplankton, demonstrating the importance of assimilating additional subsurface observations in improving the accuracy of estimated 3D fields beyond the position of the thermocline and nutricline.

To date, satellite chlorophyll, SST and SSH observations are the main observation streams for data assimilation due to their excellent spatial and temporal resolution and almost real-time accessibility for most regions of the world's oceans. Fortunately with the rapid expansion of ocean observing platforms, profiles of physical and

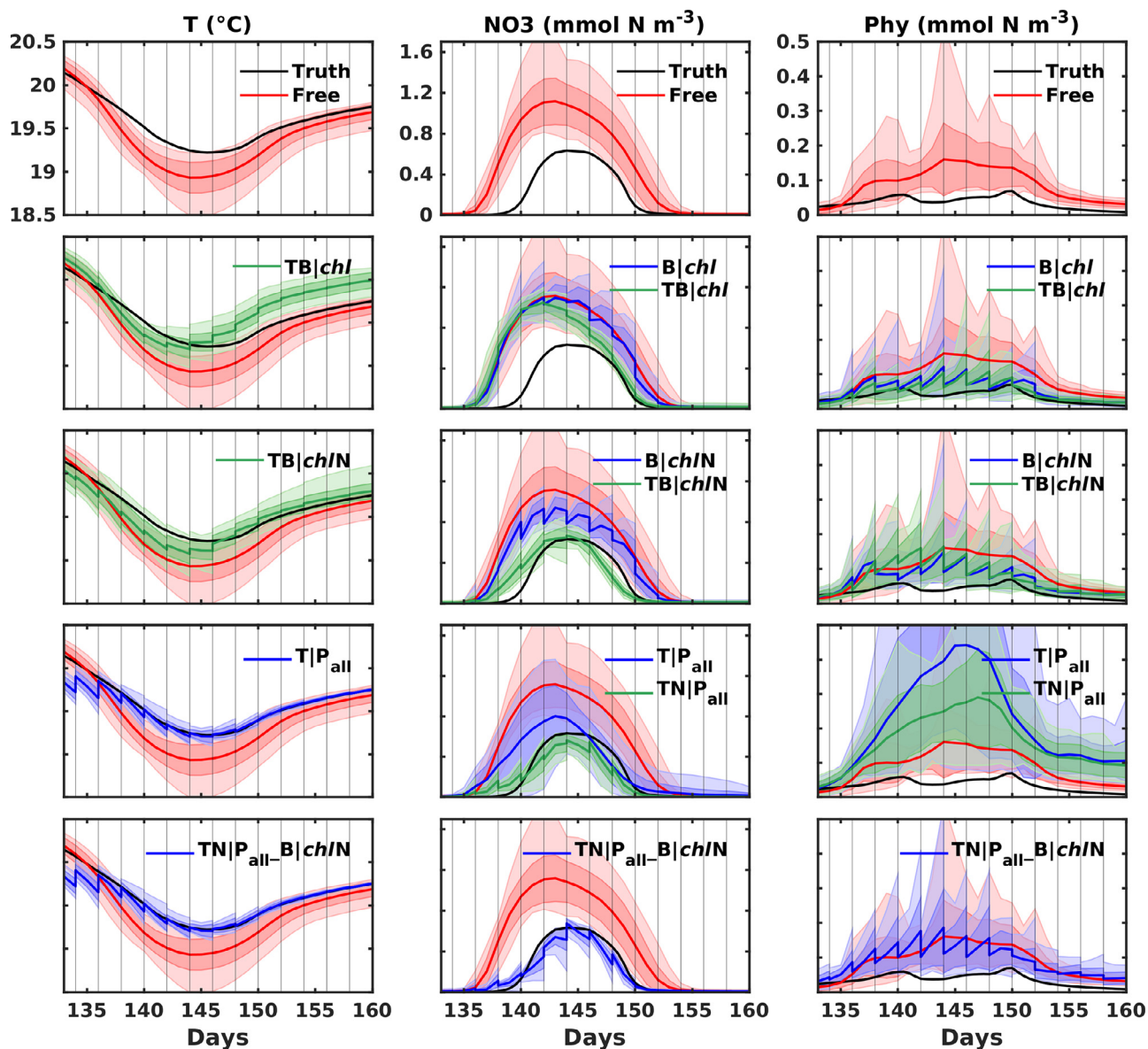


Fig. 9. Same as Fig. 2 but for the “overestimating upwelling and productivity” Scenario 2 twin experiments. (For interpretation of the references to colour in this figure legend, the reader is referred to the web version of this article.)

biogeochemical variables from floats and gliders will become more abundant and available for data assimilation to further improve model estimation and prediction.

5. Conclusions

We have assessed the impacts of updating physical and biogeochemical model fields individually versus simultaneously via different assimilation strategies on ocean ecosystem estimation and prediction. We found that adjusting the physical or biogeochemical model state alone (Method 1 “Isolated updates”) degrades the tight correlation between temperature and nitrate and is insufficient to improve biogeochemical ocean state and prediction. Simultaneous multivariate or sequential updates to physical and biogeochemical fields are required to avoid degrading the temperature and nitrate relationship and to strongly improve the biogeochemical model state. Simultaneous updates can be realized through Method 2 “Multivariate updates | single data type” by assimilating either physical or biogeochemical observations to update both model fields or Method 3 “Joint updates | both data types” that sequentially assimilates physical and biogeochemical

observations. Surface chlorophyll is of limited use for improving the 3D model state in our idealized upwelling system even when correcting physical and biogeochemical fields because the correlation between surface chlorophyll and interior nitrate and density structures is weak. This highlights the importance of collecting subsurface information for improving biogeochemical ocean model state. Overall, Method 3 “Joint updates | both data types” outperforms Method 2 “Multivariate updates | single data type” in terms of skill metrics, while Method 2 represents a capable alternative when only physical or biogeochemical observations are available.

Acknowledgments

LY acknowledges a Nova Scotia Graduate fellowship, funding from The Gulf of Mexico Research Initiative, and has benefited from a POME (Prediction and Observation of the Marine Environment) mobility grant. KF was also supported by NSERC, CFI and Compute Canada. The work contributes to the Nordic Center of Excellence EmbIA (LB and MEG). The authors would like to thank three anonymous reviewers for their constructive comments.

Supplementary materials

Supplementary material associated with this article can be found, in the online version, at doi:10.1016/j.ocemod.2018.04.005.

References

- Anderson, J.L., 2009. Spatially and temporally varying adaptive covariance inflation for ensemble filters. *Tellus Ser. A Dyn. Meteorol. Oceanogr.* 61 A, 72–83. <http://dx.doi.org/10.1111/j.1600-0870.2008.00361.x>.
- Anderson, J.L., Anderson, S.L., 1999. A Monte Carlo Implementation of the nonlinear filtering problem to produce ensemble assimilations and forecasts. *Mon. Weather Rev.* 127, 2741–2758 doi:10.1175/1520-0493(1999)127<2741:AMCIOT>2.0.CO;2.
- Anderson, L.A., Robinson, A.R., Lozano, C.J., 2000. Physical and biological modeling in the Gulf Stream region: I. Data assimilation methodology. *Deep Sea Res. Part I Oceanogr. Res. Pap.* 47, 1787–1827. [http://dx.doi.org/10.1016/S0967-0637\(00\)00019-4](http://dx.doi.org/10.1016/S0967-0637(00)00019-4).
- Berline, L., Brankart, J.-M., Brasseur, P., Ourmières, Y., Verron, J., 2007. Improving the physics of a coupled physical–biogeochemical model of the North Atlantic through data assimilation: impact on the ecosystem. *J. Mar. Syst.* 64, 153–172. <http://dx.doi.org/10.1016/j.jmarsys.2006.03.007>.
- Bierman, G.J., 1977. *Factorization Methods for Discrete Sequential Estimation*. Academic Press, New York, pp. 241.
- Burgers, G., Jan van Leeuwen, P., Evensen, G., 1998. Analysis scheme in the Ensemble Kalman Filter. *Mon. Weather Rev.* 126, 1719–1724 doi:10.1175/1520-0493(1998)126<1719:ASITEK>2.0.CO;2.
- Ciavatta, S., Torres, R., Martínez-Vicente, V., Smyth, T., Dall’Omo, G., Polimene, L., Allen, J.I., 2014. Assimilation of remotely-sensed optical properties to improve marine biogeochemistry modelling. *Prog. Oceanogr.* 127, 74–95. <http://dx.doi.org/10.1016/j.pocean.2014.06.002>.
- Ciavatta, S., Torres, R., Saux-Picart, S., Allen, J.I., 2011. Can ocean color assimilation improve biogeochemical hindcasts in shelf seas? *J. Geophys. Res. Oceans* 116, 1–19. <http://dx.doi.org/10.1029/2011JC007219>.
- Dee, D.P., 2005. Bias and data assimilation. *Q. J. R. Meteorol. Soc.* 131, 3323–3343. <http://dx.doi.org/10.1256/qj.05.137>.
- Doney, S.C., 1999. Major challenges confronting marine biogeochemical modeling. *Global Biogeochem. Cycles* 13, 705–714. <http://dx.doi.org/10.1029/1999gb900039>.
- Doney, S.C., Lindsay, K., Caldeira, K., Campin, J.-M., Drange, H., Dutay, J.-C., Follows, M., Gao, Y., Gnanadesikan, A., Gruber, N., Ishida, A., Joos, F., Madec, G., Maier-Reimer, E., Marshall, J.C., Matear, R.J., Monfray, P., Mouchet, A., Najjar, R., Orr, J.C., Plattner, G.-K., Sarmiento, J., Schlitzer, R., Slater, R., Totterdell, I.J., Weirig, M.-F., Yamanaka, Y., Yool, A., 2004. Evaluating global ocean carbon models: The importance of realistic physics. *Global Biogeochem. Cycles* 18 <http://dx.doi.org/10.1029/2003GB002150>. GB3017.
- Edwards, C.A., Moore, A.M., Hoteit, I., Cornuelle, B.D., 2015. Regional ocean data assimilation. *Annu. Rev. Mar. Sci.* 7, 21–42. <http://dx.doi.org/10.1146/annurev-marine-010814-015821>.
- Eknes, M., Evensen, G., 2002. An Ensemble Kalman Filter with a 1-D marine ecosystem model. *J. Mar. Syst.* 36, 75–100.
- Evensen, G., 1994. Sequential data assimilation with a nonlinear quasi-geostrophic model using Monte Carlo methods to forecast error statistics. *J. Geophys. Res.* 99, 10143. <http://dx.doi.org/10.1029/94JC00572>.
- Evensen, G., 2003. The Ensemble Kalman Filter: theoretical formulation and practical implementation. *Ocean Dyn.* 53, 343–367. <http://dx.doi.org/10.1007/s10236-003-0036-9>.
- Fennel, K., Losch, M., Schröter, J., Wenzel, M., 2001. Testing a marine ecosystem model: sensitivity analysis and parameter optimization. *J. Mar. Syst.* 28, 45–63. [http://dx.doi.org/10.1016/S0924-7963\(00\)00083-X](http://dx.doi.org/10.1016/S0924-7963(00)00083-X).
- Fennel, K., Wilkin, J., Levin, J., Moisan, J., O’Reilly, J., Haidvogel, D., 2006. Nitrogen cycling in the Middle Atlantic Bight: results from a three-dimensional model and implications for the North Atlantic nitrogen budget. *Global Biogeochem. Cycles* 20, 1–14. <http://dx.doi.org/10.1029/2005GB002456>.
- Fennel, K., Wilkin, J., Previdi, M., Najjar, R., 2008. Denitrification effects on air–sea CO₂ flux in the coastal ocean: simulations for the northwest North Atlantic. *Geophys. Res. Lett.* 35, 1–5. <http://dx.doi.org/10.1029/2008GL036147>.
- Fiechter, J., Broquet, G., Moore, A.M., Arango, H.G., 2011. A data assimilative, coupled physical–biological model for the Coastal Gulf of Alaska. *Dyn. Atmos. Oceans* 52, 95–118. <http://dx.doi.org/10.1016/j.dynatmoce.2011.01.002>.
- Fontana, C., Brasseur, P., Brankart, J.M., 2013. Toward a multivariate reanalysis of the North Atlantic Ocean biogeochemistry during 1998–2006 based on the assimilation of SeaWiFS chlorophyll data. *Ocean Sci.* 9, 37–56. <http://dx.doi.org/10.5194/os-9-37-2013>.
- Ford, D., Edwards, K.P., Lea, D., Barciela, R.M., Martin, M.J., Demaria, J., 2012. Assimilating GlobColour ocean colour data into a pre-operational physical–biogeochemical model. *Ocean Sci.* 8, 751–771. <http://dx.doi.org/10.5194/os-8-751-2012>.
- Ford, D., Barciela, R., 2017. Global marine biogeochemical reanalyses assimilating two different sets of remote ocean colour products. *Remote Sens. Environ.* <http://dx.doi.org/10.1016/j.rse.2017.03.040>.
- El Moussouai, A., Perruche, C., Greiner, E., Ethé, C., Gehlen, M., 2011. Integration of biogeochemistry into Mercator Ocean systems. *Mercator Océan Newsl.* 40, 3–14.
- Friedrichs, M.A.M., Dusenberry, J.A., Anderson, L.A., Armstrong, R.A., Chai, F., Christian, J.R., Doney, S.C., Dunne, J., Fujii, M., Hood, R., McGillicuddy, D.J., Moore, J.K., Schartau, M., Spitz, Y.H., Wiggert, J.D., 2007. Assessment of skill and portability in regional marine biogeochemical models: role of multiple planktonic groups. *J. Geophys. Res.* 112, C08001. <http://dx.doi.org/10.1029/2006JC003852>.
- Gaspari, G., Cohn, S.E., 1999. Construction of correlation functions in two and three dimensions. *Q. J. R. Meteorol. Soc.* 125, 723–757. <http://dx.doi.org/10.1002/qj.49712555417>.
- Geider, R., MacIntyre, H., Kana, T., 1997. Dynamic model of phytoplankton growth and acclimation: responses of the balanced growth rate and the chlorophyll a: carbon ratio to light, nutrient-limitation and temperature. *Mar. Ecol. Prog. Ser.* 148 (1), 187–200.
- Gharanti, M.E., Samuelsen, A., Bertino, L., Simon, E., Korosov, A., Daewel, U., 2017a. Online tuning of ocean biogeochemical model parameters using ensemble estimation techniques: application to a one-dimensional model in the North Atlantic. *J. Mar. Syst.* 168, 1–16. <http://dx.doi.org/10.1016/j.jmarsys.2016.12.003>.
- Gharanti, M.E., Tjiputra, J., Bethke, I., Samuelsen, A., Skjelvan, I., Bentsen, M., Bertino, L., 2017b. Ensemble data assimilation for ocean biogeochemical state and parameter estimation at different sites. *Ocean Modell.* 112, 65–89. <http://dx.doi.org/10.1016/j.ocemod.2017.02.006>.
- Ghil, M., Malanotte-Rizzoli, P., 1991. Data assimilation in meteorology and oceanography. *Adv. Geophys.* [http://dx.doi.org/10.1016/S0065-2687\(08\)60442-2](http://dx.doi.org/10.1016/S0065-2687(08)60442-2).
- Gregg, W.W., 2008. Assimilation of SeaWiFS ocean chlorophyll data into a three-dimensional global ocean model. *J. Mar. Syst.* 69, 205–225. <http://dx.doi.org/10.1016/j.jmarsys.2006.02.015>.
- Haidvogel, D.B., Arango, H., Budgell, W.P., Cornuelle, B.D., Curchitser, E., Di Lorenzo, E., Fennel, K., Geyer, W.R., Hermann, A.J., Lanerolle, L., Levin, J., McWilliams, J.C., Miller, A.J., Moore, A.M., Powell, T.M., Shchepetkin, A.F., Sherwood, C.R., Signell, R.P., Warner, J.C., Wilkin, J., 2008. Ocean forecasting in terrain-following coordinates: formulation and skill assessment of the Regional Ocean Modeling System. *J. Comput. Phys.* 227, 3595–3624. <http://dx.doi.org/10.1016/j.jcp.2007.06.016>.
- Houtekamer, P.L., Mitchell, H.L., 2001. A sequential ensemble Kalman Filter for atmospheric data assimilation. *Mon. Weather Rev.* 129, 123–137 doi:10.1175/1520-0493(2001)129<0123:ASEKFF>2.0.CO;2.
- Houtekamer, P.L., Mitchell, H.L., 1998. Data assimilation using an ensemble Kalman Filter technique. *Mon. Weather Rev.* 126, 796–811 doi:10.1175/1520-0493(1998)126<0796:DAUAEK>2.0.CO;2.
- Hu, J., Fennel, K., Mattern, J.P., Wilkin, J., 2012. Data assimilation with a local ensemble Kalman Filter applied to a three-dimensional biological model of the Middle Atlantic Bight. *J. Mar. Syst.* 94, 145–156. <http://dx.doi.org/10.1016/j.jmarsys.2011.11.016>.
- Hunt, B.R., Kostelich, E.J., Szunyogh, I., 2007. Efficient data assimilation for spatio-temporal chaos: a local ensemble transform Kalman Filter. *Phys. D Nonlinear Phenom.* 230, 112–126. <http://dx.doi.org/10.1016/j.physd.2006.11.008>.
- Jones, E.M., Baird, M.E., Mongin, M., Parslow, J., Skerratt, J., Margvelashvili, N., Matear, R.J., Wild-Allen, K., Robson, B., Rizwi, F., Oke, P., King, E., Schroeder, T., Steven, A., Taylor, J., 2016. Use of remote-sensing reflectance to constrain a data assimilating marine biogeochemical model of the Great Barrier Reef. *Biogeosciences* 13–35. <http://dx.doi.org/10.5194/bg-2016-168>.
- Kalnay, E., 2003. Atmospheric modeling, data assimilation, and predictability. *Ann. Phys.* <http://dx.doi.org/10.1256/00359000360683511>.
- Kuhn, A.M., Fennel, K., Mattern, J.P., 2015. Model investigations of the North Atlantic spring bloom initiation. *Prog. Oceanogr.* 138, 176–193. <http://dx.doi.org/10.1016/j.pocean.2015.07.004>.
- Mattern, J.P., Dowd, M., Fennel, K., 2013. Particle filter-based data assimilation for a three-dimensional physical and satellite observations. *J. Geophys. Res. Oceans* 118, 2746–2760. <http://dx.doi.org/10.1002/jgrc.20213>.
- Mattern, J.P., Song, H., Edwards, C.A., Moore, A.M., Fiechter, J., 2016. Data assimilation of physical and chlorophyll observations in the California Current System using two biogeochemical models.
- Mellor, G.L., Yamada, T., 1982. Development of a turbulence closure model for geophysical fluid problems. *Rev. Geophys.* 20, 851–875.
- Natvik, L.J., Evensen, G., 2003. Assimilation of ocean colour data into a biochemical model of the North Atlantic: part 1. Data assimilation experiments. *J. Mar. Syst.* 40–41, 127–153. [http://dx.doi.org/10.1016/S0924-7963\(03\)00016-2](http://dx.doi.org/10.1016/S0924-7963(03)00016-2).
- Oschlies, A., Garçon, V., 1999. An eddy-permitting coupled physical–biological model of the North Atlantic – 1. Sensitivity to advection numerics and mixed layer physics. *Global Biogeochem. Cycles* 13, 135–160. <http://dx.doi.org/10.1029/98gb02811>.
- Ourmières, Y., Brasseur, P., Lévy, M., Brankart, J.M., Verron, J., 2009. On the key role of nutrient data to constrain a coupled physical–biogeochemical assimilative model of the North Atlantic Ocean. *J. Mar. Syst.* 75 (1), 100–115.
- Raghukumar, K., Edwards, C.A., Goebel, N.L., Broquet, G., Veneziani, M., Moore, A.M., Zehr, J.P., 2015. Impact of assimilating physical oceanographic data on modeled ecosystem dynamics in the California Current System. *Prog. Oceanogr.* 138, 546–558. <http://dx.doi.org/10.1016/j.pocean.2015.01.004>.
- Sakov, P., Bertino, L., 2011. Relation between two common localisation methods for the EnKF. *Comput. Geosci.* 15, 225–237. <http://dx.doi.org/10.1007/s10596-010-9202-6>.
- Sakov, P., Counillon, F., Bertino, L., Lisæter, K.A., Oke, P.R., Korabely, A., 2012. TOPAZ4: an ocean-sea ice data assimilation system for the North Atlantic and Arctic. *Ocean Sci.* 8, 633–656. <http://dx.doi.org/10.5194/os-8-633-2012>.
- Sakov, P., Oke, P.R., 2008. A deterministic formulation of the ensemble Kalman Filter: an alternative to ensemble square root filters. *Tellus A* 60, 361–371. <http://dx.doi.org/10.1111/j.1600-0870.2007.00299.x>.
- Samuelsen, A., Bertino, L., Hansen, C., 2009. Impact of data assimilation of physical variables on the spring bloom from TOPAZ operational runs in the North Atlantic. *Ocean Sci.* 5, 635–647. <http://dx.doi.org/10.5194/os-5-635-2009>.
- Shulman, I., Frolov, S., Anderson, S., Penta, B., Gould, R., Sakalaukus, P., Ladner, S., 2013. Impact of bio-optical data assimilation on short-term coupled physical, bio-optical model predictions. *J. Geophys. Res. Oceans* 118, 2215–2230. <http://dx.doi.org/10.1029/2012JC008351>.

- [org/10.1002/jgrc.20177](https://doi.org/10.1002/jgrc.20177).
- Simon, E., Samuelsen, A., Bertino, L., Mouysset, S., 2015. Experiences in multiyear combined state-parameter estimation with an ecosystem model of the North Atlantic and Arctic Oceans using the Ensemble Kalman Filter. *J. Mar. Syst.* 152, 1–17. <http://dx.doi.org/10.1016/j.jmarsys.2015.07.004>.
- Song, H., Edwards, C.A., Moore, A.M., Fiechter, J., 2016a. Data assimilation in a coupled physical–biogeochemical model of the California Current System using an incremental lognormal 4-dimensional variational approach: part 2-joint physical and biological data assimilation twin experiments. *Ocean Modell.* 106, 146–158. <http://dx.doi.org/10.1016/j.ocemod.2016.04.001>.
- Song, H., Edwards, C.A., Moore, A.M., Fiechter, J., 2016b. Data assimilation in a coupled physical–biogeochemical model of the California Current System using an incremental lognormal 4-dimensional variational approach: part 3-assimilation in a realistic context using satellite and in situ observations. *Ocean Modell.* 106, 159–172. <http://dx.doi.org/10.1016/j.ocemod.2016.04.001>.
- Wilson, C., Adamec, D., 2002. A global view of bio-physical coupling from SeaWiFS and TOPEX satellite data, 1997–2001. *Geophys. Res. Lett.* 29, 1–4. <http://dx.doi.org/10.1029/2001GL014063>.
- While, J., Haines, K., Smith, G., 2010. A nutrient increment method for reducing bias in global biogeochemical models. *J. Geophys. Res. Oceans* 115 (C10).
- Xue, Z., He, R., Fennel, K., Cai, W.J., Lohrenz, S., Hopkinson, C., 2013. Modeling ocean circulation and biogeochemical variability in the Gulf of Mexico. *Biogeosciences* 10, 7219–7234. <http://dx.doi.org/10.5194/bg-10-7219-2013>.